Research Article | Vol. 26, No. 8 | 16 Apr 2018 | OPTICS EXPRESS 9714
Optics EXPRESS

Characterization of a fully integrated heterogeneous silicon/III-V colliding pulse mode-locked laser with on-chip feedback

SONGTAO LIU,[1,*] TIN KOMLJENOVIC,[1] SUDHARSANAN SRINIVASAN,[2] ERIK NORBERG,[2] GREGORY FISH,[2] AND JOHN E. BOWERS[1]

[1]*Department of Electrical and Computer Engineering, University of California, Santa Barbara, CA 93106 USA*
[2]*Juniper Networks, Goleta, CA 93117, USA*
[*]*songtao_liu@ucsb.edu*

Abstract: A fully integrated heterogeneous silicon/III-V colliding pulse mode-locked laser with tunable on-chip optical feedback operating in the O-band is extensively investigated. The 19-GHz colliding pulsed laser operates in a wide mode-locking regime with good mode locking quality. By precisely controlling the strength and phase of the on-chip optical feedback signal, the laser exhibits clear periodic pulse shortening effects. The RF 3 dB linewidth was reduced by a factor of 4.7 down to 6 kHz, as compared to the free running state.

OCIS codes: (140.4050) Mode-locked lasers; (250.5300) Photonic integrated circuits; (250.5960) Semiconductor lasers.

References and links

1. J. Sun, E. Timurdogan, A. Yaacobi, E. S. Hosseini, and M. R. Watts, "Large-scale nanophotonic phased array," Nature **493**(7431), 195–199 (2013).
2. T. J. Seok, N. Quack, S. Han, R. S. Muller, and M. C. Wu, "Large-scale broadband digital silicon photonic switches with vertical adiabatic couplers," Optica **3**(1), 64–70 (2016).
3. D. Pérez, I. Gasulla, L. Crudgington, D. J. Thomson, A. Z. Khokhar, K. Li, W. Cao, G. Z. Mashanovich, and J. Capmany, "Multipurpose silicon photonics signal processor core," Nat. Commun. **8**(1), 1–9 (2017).
4. D. Liang and J. E. Bowers, "Recent progress in lasers on silicon," Nat. Photonics **4**(8), 511–517 (2010).
5. G. Roelkens, L. Liu, D. Liang, R. Jones, A. Fang, B. Koch, and J. Bowers, "III-V/silicon photonics for on-chip and intra-chip optical interconnects," Laser Photonics Rev. **4**(6), 751–779 (2010).
6. C. Zhang, S. Zhang, J. D. Peters, and J. E. Bowers, "8 × 8 × 40 Gbps fully integrated silicon photonic network on chip," Optica **3**(7), 785 (2016).
7. A. Spott, E. J. Stanton, N. Volet, J. D. Peters, J. R. Meyer, and J. E. Bowers, "Heterogeneous Integration for Mid-infrared Silicon Photonics," IEEE J. Sel. Top. Quantum Electron. **23**(6), 1–10 (2017).
8. H. G. Weber, R. Ludwig, S. Ferber, C. Schmidt-Langhorst, M. Kroh, V. Marembert, C. Boerner, and C. Schubert, "Ultrahigh-speed OTDM-transmission technology," J. Lightwave Technol. **24**(12), 4616–4627 (2006).
9. K. A. Williams, M. G. Thompson, and I. H. White, "Long-wavelength monolithic mode-locked diode lasers," New J. Phys. **6**, 1–30 (2004).
10. S. Liu, H. Wang, M. Sun, L. Zhang, W. Chen, D. Lu, L. Zhao, R. Broeke, W. Wang, and C. Ji, "AWG-Based Monolithic 4×12 GHz Multichannel Harmonically Mode-Locked Laser," IEEE Photonics Technol. Lett. **28**(3), 241–244 (2016).
11. J. H. Marsh and L. Hou, "Mode-locked laser diodes and their monolithic integration," IEEE J. Sel. Top. Quantum Electron. **23**(6), 1 (2017).
12. K. Yvind, D. Larsson, L. J. Christiansen, C. Angelo, L. K. Oxenløwe, J. Mørk, D. Birkedal, J. M. Hvam, and J. Hanberg, "Low-jitter and high-power 40-GHz all-active mode-locked lasers," IEEE Photonics Technol. Lett. **16**(4), 975–977 (2004).
13. L. Hou, M. Haji, J. H. Marsh, and A. C. Bryce, "10 GHz AlGaInAs/InP 1.55 μm passively mode-locked laser with low divergence angle and timing jitter," Opt. Express **19**(26), B75–B80 (2011).
14. M. L. Davenport, S. Member, S. Skendžić, N. Volet, J. C. Hulme, S. Member, M. J. R. Heck, and J. E. Bowers, "Heterogeneous Silicon / III-V Semiconductor Optical Amplifiers," IEEE J. Sel. Top. Quantum Electron. **22**(6), 3100111 (2016).
15. M. Haji, L. Hou, A. E. Kelly, J. Akbar, J. H. Marsh, J. M. Arnold, and C. N. Ironside, "High frequency optoelectronic oscillators based on the optical feedback of semiconductor mode-locked laser diodes," Opt. Express **20**(3), 3268–3274 (2012).

#323357 https://doi.org/10.1364/OE.26.009714
Journal © 2018 Received 15 Feb 2018; revised 26 Mar 2018; accepted 28 Mar 2018; published 4 Apr 2018

Optics EXPRESS

16. M. Passerini, M. Sorel, P. J. R. Laybourn, G. Giuliani, and S. Donati, "Semiconductor colliding-pulse mode-locked lasers at 60 GHz subjected to optical feedback," Proc. SPIE **5452**, 146 (2004).
17. O. Solgaard and K. Y. Lau, "Optical Feedback Stabilization of the Intensity Oscillations in Ultrahigh-Frequency Passively Modelocked Monolithic Quantum-Well Lasers," IEEE Photonics Technol. Lett. **5**(11), 1264–1267 (1993).
18. C. Y. Lin, F. Grillot, N. A. Naderi, Y. Li, and L. F. Lester, "Rf linewidth reduction in a quantum dot passively mode-locked laser subject to external optical feedback," Appl. Phys. Lett. **96**(5), 94–97 (2010).
19. H. Asghar and J. G. McInerney, "Asymmetric dual-loop feedback to suppress spurious tones and reduce timing jitter in self-mode-locked quantum-dash lasers emitting at 1.55 μm," Opt. Lett. **42**(18), 3714–3717 (2017).
20. M. L. Davenport, S. Srinivasan, M. J. R. Heck, and J. E. Bowers, "A Hybrid Silicon / InP Integrated Feedback Stabilized Mode- Locked Laser," in *Opt. Fiber Commun. Conf.* (2014), pp. 8-10.
21. S. Srinivasan, E. Norberg, T. Komljenovic, M. Davenport, G. Fish, and J. E. Bowers, "Hybrid Silicon Colliding-Pulse Mode-Locked Lasers with On-Chip Stabilization," IEEE J. Sel. Top. Quantum Electron. **21**(6), 24–29 (2015).
22. T. Thiessen and J. K. S. Poon, "20 GHz Mode-Locked Laser Diodes with Integrated Optical Feedback Cavities in a Generic Monolithic InP Photonics Platform," IEEE Photonics J. **9**(5), 1–10 (2017).
23. A. W. Fang, H. Park, O. Cohen, R. Jones, M. J. Paniccia, and J. E. Bowers, "Electrically pumped hybrid AlGaInAs-silicon evanescent laser," Opt. Express **14**(20), 9203–9210 (2006).
24. E. A. Avrutin and B. M. Russell, "Dynamics and spectra of monolithic mode-locked laser diodes under external optical feedback," IEEE J. Quantum Electron. **45**(11), 1456–1464 (2009).
25. T. Komljenovic, S. Liu, E. Norberg, G. A. Fish, and J. E. Bowers, "Control of Widely Tunable Lasers With High-Q Resonator as an Integral Part of the Cavity," J. Lightwave Technol. **35**(18), 3934–3939 (2017).
26. D. J. Derickson, R. J. Helkey, A. Mar, J. R. Karin, J. G. Wasserbauer, and J. E. Bowers, "Short pulse generation using multisegment mode-locked semiconductor lasers," IEEE J. Quantum Electron. **28**(10), 2186–2202 (1992).
27. L. A. Coldren, S. W. Corzine, and M. L. Mašanović, "Dynamic Effects," in *Diode Lasers and Photonic Integrated Circuits* (John Wiley & Sons, Inc., 2012), pp. 247–333.
28. D. A. Ackerman, L. M. Zhang, L. J. P. Ketelsen, and J. E. Johnson, "Characterizing residual reflections within semiconductor lasers, integrated sources, and coupling optics," IEEE J. Quantum Electron. **34**(7), 1224–1230 (1998).
29. H. Simos, C. Simos, C. Mesaritakis, and D. Syvridis, "Two-section quantum-dot mode-locked lasers under optical feedback: Pulse broadening and harmonic operation," IEEE J. Quantum Electron. **48**(7), 872–877 (2012).
30. O. Nikiforov, L. Jaurigue, L. Drzewietzki, K. Lüdge, and S. Breuer, "Experimental demonstration of change of dynamical properties of a passively mode-locked semiconductor laser subject to dual optical feedback by dual full delay-range tuning," Opt. Express **24**(13), 14301–14310 (2016).
31. D. Lenstra, B. Verbeek, and A. Den Boef, "Coherence collapse in single-mode semiconductor lasers due to optical feedback," IEEE J. Quantum Electron. **21**(6), 674–679 (1985).
32. S. Rauch, L. Drzewietzki, A. Klehr, J. Sacher, W. Elsäßer, and S. Breuer, "Experimental Study of the Timing Hitter of a Passively Mode-Locked External-Cavity Semiconductor Laser Subject to Repetition Rate Transitions and Optical Feedback," IEEE J. Quantum Electron. **51**(4), 1–7 (2015).
33. M. J. R. Heck, J. F. Bauters, M. L. Davenport, D. T. Spencer, and J. E. Bowers, "Ultra-low loss waveguide platform and its integration with silicon photonics," Laser Photonics Rev. **8**(5), 667–686 (2014).

1. Introduction

Silicon photonics uses well-established silicon processing, packaging and testing technology to increase the complexity of photonic integrated circuits (PICs) for applications, such as advanced 5G communication systems, next generation data centers, the Internet of Things, and advanced automotive radar systems [1–6]. Based on the high index contrast, low propagation loss silicon-on-insulator (SOI) waveguide platform, a wide variety of large scale silicon PICs have been demonstrated, such as two-dimensional photonic phased arrays [1], broadband silicon photonic switches [2], and multipurpose optical signal processors [3]. It is preferable to further integrate lasers and amplifiers within the large-scale silicon PICs. However, due to the indirect bandgap of Si, the lasing efficiency is extremely low compared to its III/V counterparts [4]. Recent research has demonstrated different approaches to address this problem [5]. Among them, wafer bonding technology shows great flexibility for integrating lasers at wavelengths from near-infrared to middle-infrared [7]. The highest level of integration in a heterogeneously integrated photonic chip with 440 active and passive components was demonstrate by Chong et al. [6].

Future advanced applications put higher requirements on bandwidth, transmission speed, and power consumption. Wavelength-division multiplexing (WDM) is the most straightforward way to improve the PIC capacity [6]. Mode-locked lasers are attractive WDM

Optics EXPRESS

sources in terms of footprint, control simplicity and power consumption, as they can generate broadband optical spectrum of multiple phase-correlated laser lines with a fixed spacing that is defined by the cavity length. In addition, high speed short pulse generation in the time domain makes them a promising candidate in time-division multiplexing (TDM) systems [8]. Other applications are interchip/intrachip clock distribution, arbitrary waveform generation, millimeter wave signal generation, high-speed photonic analog-to-digital conversion [9,10].

Passively mode-locked lasers can emit high speed pulses from several gigahertz up to terahertz without the need of an external RF modulation signal [11]. However, due to the absence of a synchronized timing source, the lasers suffer significant pulse to pulse timing jitter originated mainly from amplified spontaneous emission (ASE) noise, which is also reflected on the broad RF linewidth [12]. One way to suppress the ASE noise is to lower the optical confinement factor Γ in order to reduce the amount of ASE noise coupled to the oscillating mode [12, 13]. Based on the wafer bonding technique, it is quite easy to control the confinement factor by varying the III/V gain length and the silicon waveguide width, which offers great design flexibility [14]. An alternative method is to deploy an external feedback cavity to store the coherent photon energy and feed a small portion of light back into the cavity to suppress the ASE noise, which can also help to enhance the mode-locking quality, leading to large RF linewidth reduction [15–19]. However, previously reported free space or fiber loop based optical feedback (OFB) configurations suffer from mechanical and thermal instabilities due to bulk components, which will compromise the performance of the laser in long term stability and add complexity for full integration. Monolithic integration with an on-chip feedback cavity, on the contrary, offers the opportunity to get rid of all the external optical bulk components, such as lenses, mirrors, polarization controllers, and attenuators [20–22]. Their small form factor, power efficiency, and possibility to integrate with other components make them promising in chip level integration within large scale PICs.

In this paper, we demonstrate a fully integrated 19 GHz colliding pulse mode-locked semiconductor laser (CPMSL) with tunable on-chip feedback by leveraging CMOS compatible heterogeneous silicon platform that provides low loss SOI waveguides and efficient light generation via bonding high-quality III/V material [23]. Benefiting from the low loss Si waveguide, no extra semiconductor optical amplifier (SOA) in the feedback cavity is needed, which simplifies the feedback signal control as well as eliminating the excess ASE noise introduced by the SOA. The length of the on-chip external cavity is designed to be twice the laser fundamental cavity length to realize resonant feedback [24]. The on-chip external cavity contains two phase tuners, one of which is placed in one arm of the interferometer, for controlling the OFB signal strength and the other in the feedback cavity to further adjust the OFB phase. 4.7x improvement of RF linewidth as well as pulsewidth shortening can be obtained by precisely tuning the feedback signal strength and phase. This monolithically integrated CPMSL chip employs loop mirrors that can fully take advantage of high resolution optical lithography to precisely define the fundamental cavity length and remove the cleave uncertainty once and for all, enabling further integration within more complex PICs.

2. CPMSL chip design

Figure 1 shows the schematic diagram of the fully integrated heterogeneous CPMSL with on-chip optical feedback cavity. The CPMSL was fabricated using a heterogeneous silicon/III-V wafer bonding photonic integration process [25]. The colliding pulse mode-locking design cavity, which is formed by two loop mirrors, has a cavity length of 3.94 mm, corresponding to a fundamental mode-locking frequency of ~9.6 GHz. The saturable absorber (SA) section is positioned at the middle of the cavity, enabling second harmonic mode locking operation. The total gain section length is 1200 μm, the SA length is 40 μm with two 15 μm isolation trenches in between the gain and SA section. The reflectivities of front and back loop mirrors are 15% and 85%, respectively. The output port connecting to the front mirror is 7° angled to

Optics EXPRESS

minimize unintentional reflections. By introducing an external cavity connected through the back-loop mirror, the optical feedback mechanism can be realized on chip. The total length of the feedback cavity is designed to be twice the fundamental cavity, and comprises two thermal phase tuners, a 2 × 2 multimode interferometer (MMI), two 1 × 2 MMIs and a monitor photodiode (MPD), which has a responsivity of ~0.85 A/W. It is terminated by two 100% reflectivity loop mirrors. By thermally tuning the phase of one of the aforementioned loop mirrors in the external cavity, the interference condition inside the 2 × 2 MMI can be controlled precisely, leaving the OFB strength carefully controlled and simultaneously monitored by the MPD. Combined with the control of the feedback cavity phase, the final mode-locking quality can be improved, leading to the anticipated cavity noise suppression and RF linewidth reduction. The gain, SA section and the MPD share the same III/V material and were wafer bonded onto the top of the pattered SOI waveguide. The silicon waveguide propagation loss is below 2 dB/cm. The total chip size is approximately 3.7 mm × 0.7 mm.

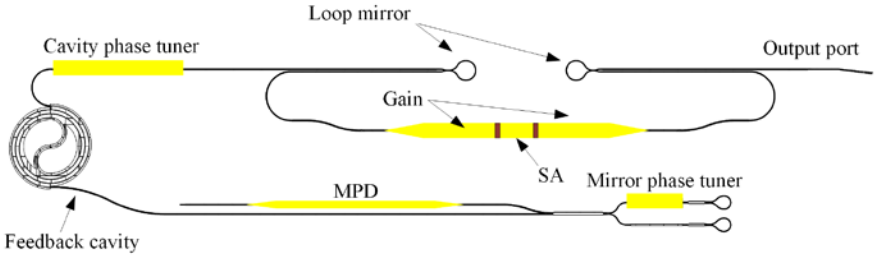

Fig. 1. A schematic diagram of the heterogeneously integrated colliding pulse mode-locked laser with on-chip feedback cavity. SA: saturable absorber, MPD: monitor photodiode.

3. Experimental results and discussion

The fabricated CPMSL chip was tested on a copper heatsink with a fixed stage temperature of 20.ºC A probe card with combined RF ground signal (GS) and DC contacts was used to facilitate the passive mode locking test. The optical output signal was collected by a 2-μm single mode anti-reflection coated lensed fiber. Due to the angled output waveguide of the chip, the fiber boat was placed 23º tilted to the normal of the cleaved facet to maximize the coupling efficiency (coupling loss around 6 - 7 dB). The signal was then split and routed to an optical spectrum analyzer (Yokogawa, AQ6370C), an electronic spectrum analyzer (50-GHz u^2t photodiode with Rohde&Schwarz, FSU) and an autocorrelator (Femtochrome, FR-103MN) for optical spectrum, frequency domain and time domain autocorrelation analysis, respectively.

3.1 Laser basic characteristics without on-chip feedback

The fiber coupled output power and dynamic resistance as a function of forward gain section current of the CPMSL under different reverse biased voltage (two phase sections left floating) were first characterized, as shown in Fig. 2(a). It can be seen clearly that the threshold current of the laser increased gradually from 31 mA to 42 mA when the bias on the SA is ramped from 0 V to –2 V with a step of 0.5 V. The slope efficiency as well as the maximum coupled output power also decreased due to the increased absorption in the reverse biased SA section. The dynamic resistance (dV/dI) curve of the chip under different SA bias is also plotted in Fig. 2(a). A sharp drop in resistance corresponding to the beginning of lasing can be observed due to carrier density clamping effect. The drop point follows the increase of the threshold. The series resistance was constant at slightly below 3 Ω after the laser started lasing.

The passive colliding pulse mode locking area of the CPMSL was then investigated by sweeping the forward biased gain section current and reverse biased SA section voltage (two phase section of the on-chip feedback cavity left floating). The criterion to decide a good mode locking state is restricted to the corresponding second harmonic frequency tone’s signal

Optics EXPRESS

to noise (SNR) ratio larger than 30 dB with pulse width narrower than 5 ps. As exhibited in Fig. 2(b), a wide mode locking area is obtained under the aforementioned criterion with forward current ranging from 60 mA to 160 mA and reverse voltage ranging from 0.2 V to 1.8 V. For most recorded mode locking points, the 2nd RF peak SNR ratio is larger than 50 dB. The corresponding pulse mapping diagram is presented in Fig. 2(c). It is interesting to note that narrower pulses occurred at lower current and reverse voltage bias. The time-bandwidth product (TBP) under these conditions tend to be close to the transform limited value (not shown in the graph), suggesting effective pulse shaping mechanism between the gain and SA section [26]. Increasing the gain and SA bias leads the pulse to experience more self-phase modulation that adds chirping to the pulse, resulting in larger TBP. The narrowest pulse is obtained at I_{gain} = 90 mA, V_{SA} = - 0.6 V, which is shown in Fig. 2(d). The pulsewidth is 1.9 ps when fit to a hyperbolic secant squared pulse profile. Full width half maximum of the corresponding spectrum shown in Fig. 2(e) is 1.1 nm, leading to a nearly transform limited TBP value of 0.37. Figure 2(f) gives the frequency performance of the laser in a 50-GHz span view. A sharp RF peak with a SNR > 60 dB at the second harmonic frequency tone around 19.2 GHz with its higher order harmonic can be seen. The fundamental frequency of the laser is suppressed perfectly, showing excellent colliding pulse mode locking quality.

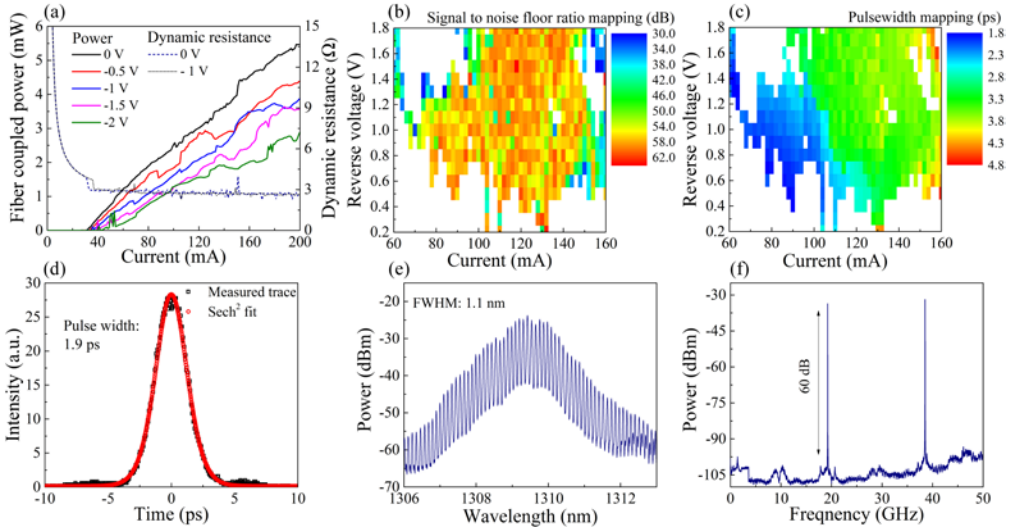

Fig. 2. (a) fiber coupled output power and dynamic resistance as a function of gain section current under different SA reverse bias, (b) second harmonic RF peak signal to noise ratio mapping, (c) pulsewidth mapping of the CPMSL laser, (d) measured pulse autocorrelation trace with sech^2 fit, (e) optical spectrum, (f) 50-GHz span frequency spectrum of the CPMSL laser under narrowest pulse generation condition (I_{gain} = 90 mA, V_{SA} = - 0.6 V), both on-chip feedback cavity phase section left floating, T_{stage} = 20°C.

Optics EXPRESS

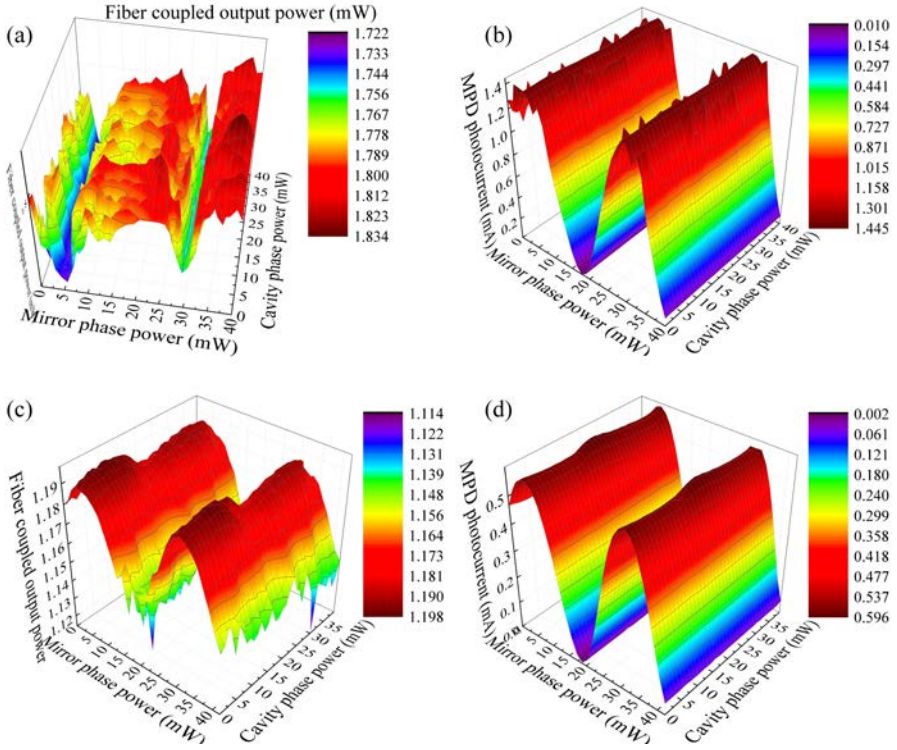

Fig. 3. The CPMSL chip (a) fiber coupled output power and (b) MPD photocurrent mapping under CW mode with gain section and SA section forward biased together at 150 mA, (c) fiber coupled output power and (d) MPD photocurrent mapping under narrowest pulse generation mode locking state (I_{gain} = 90 mA, V_{SA} = - 0.6 V) as a function of mirror phase power and cavity phase power, T_{stage} = 20°C.

3.2 Laser performance with on-chip feedback

3.2.1 Output power

The characterization of the performance of the laser with on-chip resonant optical feedback was then carried out. Intuitively, the output power should increase when the OFB is injected into the fundamental cavity, as is the case shown in Figs. 3(a) and 3(b), where the laser was operated under continuous wave (CW) mode as a traditional Fabry-Perot (FP) laser with gain and SA section forward biased together at 150 mA. Thermally tuning the mirror phase section on one arm of the 2 × 2 MMI changes the internal interference condition and varies the power ratio between the two output ports, one connected to the MPD, the other connected to the feedback cavity, leading to the precisely controlled OFB power. From Figs. 3(a) and 3(b), it is found that when tuning the mirror phase to around 5 mW and 30 mW, all the optical power in the feedback cavity goes into the MPD, the photocurrent increases to its maximum, while the output power of the laser goes down to their local minimum. In between the two minima, the output power of the laser varies randomly and independent of the cavity phase section tuning. However, the laser exhibits distinct characteristics when it operates in a mode locked (ML) state. Figures 3(c) and 3(d) present the 3D mapping diagrams of the fiber coupled output power and MPD photocurrent of the CPMSL under minimum pulsewidth condition (I_{gain} = 90 mA, V_{SA} = - 0.6 V), respectively. It is clear to see that periodic variation of fiber coupled output power and MPD photocurrent are both dependent on mirror phase power (MPP) and cavity phase power (CPP). Although the output power variation is small (around 0.06 mW), it is opposite to the FP case. The output power of the ML case reaches its maximum in accordance with the MPD photocurrent, and decreases with the decrease of the

Optics EXPRESS

photocurrent. This means more OFB power injected into the fundamental cavity, less output power collected by the fiber. The explanation behind this phenomenon lies in the coherent feedback mechanism [27]. With on-chip feedback, the accumulated round-trip phase of each lasing mode under feedback must satisfy the cavity resonance condition. Stronger feedback along with carrier density change allows multiple potential modes possible around each original fundamental cavity mode. Among those modes, the one with closest to the in-phase reinjection condition can obtain the lowest threshold gain and become the dominant mode in the spectrum. However, due to chromatic dispersion effect in the waveguide, not all the modes in the OFB wave packet can be tuned to realize in-phase reinjection to the fundamental cavity, which means modes near in-phase feedback condition are preferred, while the other modes are forced to suffer higher threshold gain due to phase locked property of mode-locked lasers. This effect manifests lasing wavelength shift as well as peak wavelength change as shown in Fig. 4(d) when the MPP is tuned from 4.5 mW (minimum OFB) to 18.4 mW (close to maximum OFB). Under this case, modes on the shorter wavelength side show resonance enhancement while modes on the other side are weakened. A huge periodic suppression of particular certain modes also can be seen along the wavelength span in Fig. 4(d), indicating those modes are far away from the in-phase feedback condition that suffer from the highest threshold gain. Greater the OFB power, bigger suppression is exhibited. The total effects lead to the output power decrease with the increase of the OFB power. This is in contradictory to the FP case, where random phase relationship exhibits among these lasing modes that all the modes could be selected at their lowest threshold gain, leading to an overall increased output power under OFB albeit without periodicity. Power integrals of the mode-locked spectra further validate the descending trend on the fiber coupled output power with increase of the OFB strength. Varying the cavity phase section power, on the other direction, changes the phase of the OFB signal periodically. Consequently, those modes which has the lowest threshold gain can again be dominant, leading to a change of the output spectrum accordingly as shown in Fig. 4(e), as well as the less prominent periodic variation of the output power. An estimation of the on chip feedback cavity length was done by employing the method proposed in [28], where a Fourier transform of the subthreshold optical spectra of the laser (gain and SA section forward biased together at 20 mA) from the wavevector to the length domain was carried out. The results show that the laser feedback cavity length design is slightly shorter than the desired integer value of two times, which, however, wouldn't affect the resonant condition as the range of feedback cavity length for the resonant regime is relatively broad, especially when the operating point is several times larger than the threshold (in this case, around 3x) [17,24]. We would like to point out that the laser actually always has some level of on-chip OFP even if the MPP is zero, which is caused by the fabrication variation of the 2 $\times$ 2 MMI leading to slight power splitting ratio deviation.

3.2.2 Pulsewidth

The pulsewidth evolution as a function of MPP and CPP is shown in Fig. 4(a). Clearly regular pulse evolving pattern can be observed under the strength and phase tuning of the OFB signal. Two cross-sections of the pulsewidth and MPD photocurnent under fixed CPP (8 mW) and fixed MPP (18.4 mW) are exhibited in Figs. 4(b) and 4(c), respectively, to elucidate the influence of the OFB signal. Generally, from Fig. 4(b), it can be found that the pulsewidth varies periodically as the same trend as the variation of the MPD photocurrent, suggesting more OFB power, narrower the pulse. Pulsewidth broadens at strongest OFB power around MPP 17.5 mW. This result is in a good agreement with the numerical analysis in [29], indicating our resonant feedback cavity design is quite accurate. A comparison of the corresponding spectra under maximum pulsewidth (2.06 ps, CPP: 8 mW, MPP: 4.5 mW) and minimum pulsewidth (1.83 ps, CPP: 8 mW, MPP: 18.4 mW) condition is plotted in Fig. 4(d). It shows a clear spectral change with the increase of the OFB power due to the aforementioned coherence feedback mechanism. Under this case, due to the suppression of

Optics EXPRESS

the center wavelength, side modes can share more gain thus increase the effective 3 dB spectral bandwidth. This leads to the corresponding pulsewidth reduction as shown in Fig. 4(f). The occurrence of the side lobes is caused by the periodic mode suppression effect exhibited in the spectrum. Tuning the cavity phase section power further modifies the phase of the OFB signal, leading to the periodic variation of the coherent resonance condition between fundamental cavity modes with OFB signal. This, in turn, influences the spectral 3 dB effective bandwidth periodically, as shown in Fig. 4(e), giving rise to the corresponding periodic variation of the pulsewidth as presented in Fig. 4 (c). More theoretical modelling work on spectrum and pulse shape variation needs to be done to further justify this phenomenon, and will be reported in a future publication.

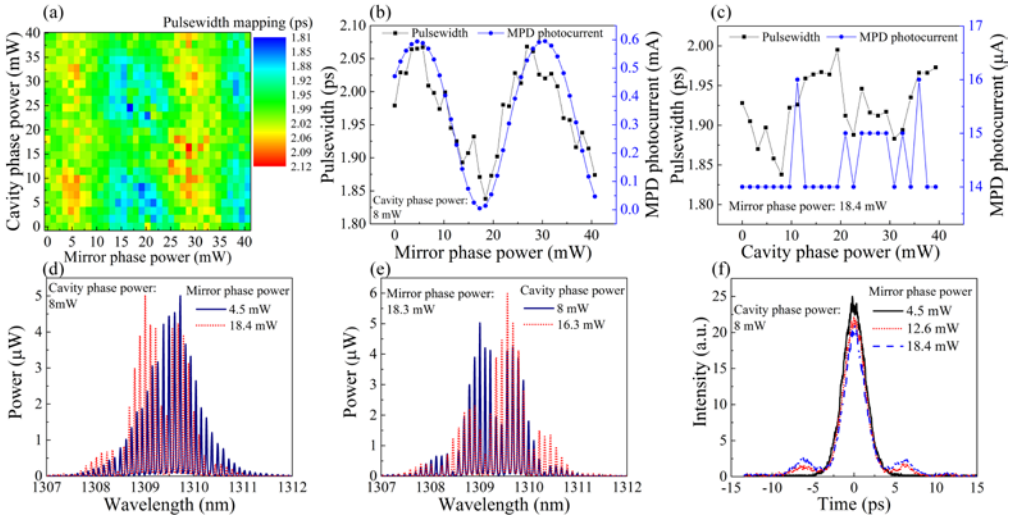

Fig. 4. (a) pulsewidth mapping as a function of mirror phase power and cavity phase power, (b) pulsewidth and MPD photocurrent as a function of mirror phase power under fixed cavity phase power (8 mW), (c) pulsewidth and MPD photocurrent as a function of cavity phase power under fixed mirror phase power (18.4 mW), (d) spectrum comparison under different mirror phase power, (e) spectrum comparison under different cavity phase power, (f) pulse trace evolution under different mirror phase power (I_{gain} = 90 mA, V_{SA} = - 0.6 V, T_{stage} = 20°C).

3.2.3 RF 3 dB linewidth

RF linewidth measurement of the CPMSL with on-chip OFB is then followed by changing the phase section bias sources to low noise battery sources (ILX LDX-5620B) to get isolation from wall plug power due to the laser sensitivity to external noise. The gain and SA section were biased by linear current and voltage sources due to the limit number of battery sources at the moment. The GS probe was also employed to measure the second harmonic RF signal directly from the SA section. Figure 5(a) shows the RF 3 dB linewidth evolution as a function of the MPP and CPP. Blue shaded squares represent the preferable phase section operation conditions where narrow RF 3 dB linewidth can be obtained. Less regular evolving pattern than that of the pulse evolution mapping diagram can be observed caused by the excess noise, but we can still recognize that with the help of the RF peak mapping diagram shown in Fig. 5(b). It can be observed from Fig. 5(b) that the colliding pulse repetition frequency of the laser increase with the increase of the OFB pulse strength (MPP: ~4.5 mW to ~17.5 mW). It indicates the effective index of the fundamental cavity decrease due to stronger OFB signal reinjection, corresponding to the wavelength shift effect shown in Fig. 4(d). The RF peak also exhibit periodical variation due to its self-adaption to the OFB reinjected pulses [30], which have a leading or trailing position compared to the unperturbed fundamental cavity pulses that introduced by cavity phase section periodic tuning. When comparing the two mapping graphs,

Optics EXPRESS

it is interesting to note that narrower RF linewidth points are mostly occurred at conditions where the laser operating frequency is around its natural mode locking rate under on-chip OFB (blue shaded areas under weak OFB from MPP 0 mW to around 7.5 mW and green shaded areas under strong OFB from MPP around 11 mW to 16 mW, frequency deviation within this area is below 5 MHz). The missing points in Fig. 5(a) around MPP 17.5 mW indicate the RF 3 dB linewidth is larger than 100 kHz. This corresponds to a maximum OFB reinjection power on the order of –11 dBm when taking MPD's responsivity, waveguide loss and back mirror reflectivity into consideration. This phenomenon combined with the pulsewidth rebroadening behavior at strongest on-chip OFB power suggest the mode locked laser operation status might be close to its own coherence collapse region [31]. The narrowest RF 3 dB linewidth of 6 kHz is obtained around MPP 15 mW and CPP 25 mW as shown in Fig. 5(c) when fitting to a Voigt function. Comparing with the 28 kHz RF 3 dB linewidth of the chip without on-chip OFB around MPP 4.5 mW, a reduction factor of 4.7 is obtained. Corresponding timing jitter under this state is 1.2 ps, integrated from 100 kHz to 100 MHz. Packaging of the laser is expected to improve the laser long-term stability.

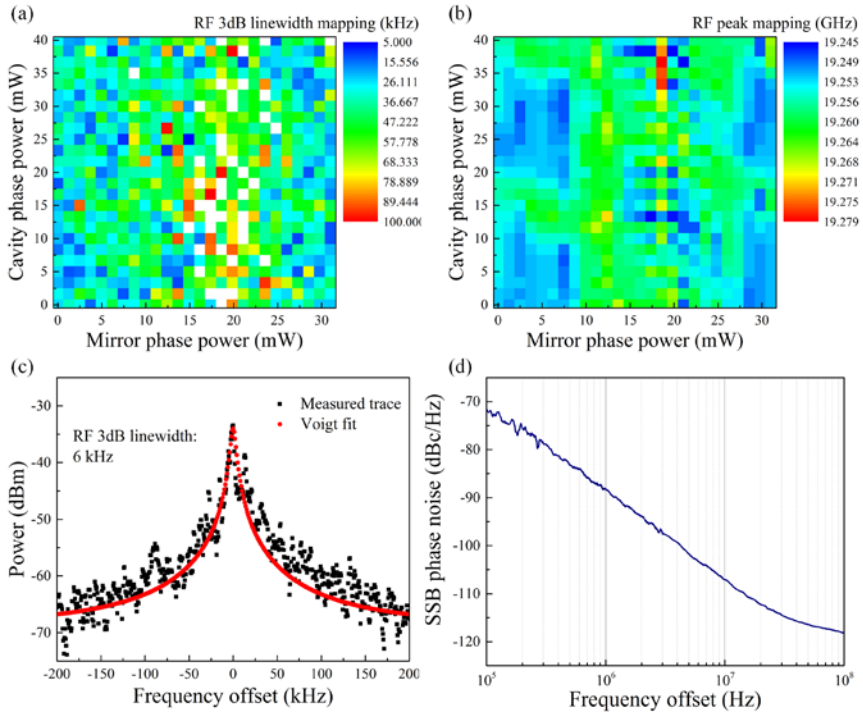

Fig. 5. (a) RF 3 dB linewidth and (b) second harmonic repetition frequency mapping as a function of mirror phase power and cavity phase power, (c) narrowest RF 3 dB linewidth (RF peak occurred at 19.26 GHz) and (d) corresponding single-sideband phase noise plot (I_{gain} = 90 mA, V_{SA} = - 0.6 V, mirror phase power: 15 mW, cavity phase power: 25 mW, T_{stage} = 20°C).

A further comparison with single fiber loop based OFB mechanism was investigated by biasing the laser without on-chip feedback (bias condition same as above). The fiber loop length is around 23 m according to the side mode spacing exhibited in the frequency spectrum, including circulator, coupler, polarization controller, praseodymium doper fiber amplifier, etc. A striking RF 3 dB linewidth reduction down to 766 Hz (fitted by the Voigt function) can be obtained under feedback power around – 4.4 dBm (power reflected to the front facet monitored by power meter). This is expected because the longer OFB cavity length (within the coherence length) and the stronger OFB power give a better noise suppression and RF linewidth reduction [32]. However, multiple supermode noise resonances with frequency

Optics EXPRESS

spacing corresponding to the fiber loop length occurred around the main mode locking frequency can compromise the practicability of the laser. Although dual fiber loop configuration can address this issue to some extent, its stability further limits practical applications [15]. Our monolithically integrated CPMSL chip with on-chip feedback cavity has demonstrated its precise control on OFB strength and phase with better stability performance. Future dual on-chip feedback cavity can be designed to further improve the RF performance. Integration of long ultralow loss silicon nitride waveguide with propagation loss below 0.1 dB/m is also preferable [33].

4. Conclusion

In conclusion, we have thoroughly characterized and analyzed an O-band 19 GHz colliding pulse mode locked laser with on-chip resonant optical feedback mechanism built on the silicon heterogeneous integration platform. The laser exhibits wide mode locking area with excellent mode locking quality. By tuning the strength and phase of the on chip OFB signal, clear pulse shortening from 2.06 ps down to 1.83 ps and RF 3 dB linewidth reduction from 28 kHz down to 6 kHz are demonstrated. These results set new records for a fully integrated CPMSL on silicon operating in the O-band. Future designs incorporating a dual on-chip feedback cavity configuration and ultralow loss silicon nitride waveguide could further improve the laser performance. On-chip generation of tens of gigahertz high repetition rate pulses with 3 dB RF linewidth down to sub-kilohertz is anticipated. The excellent performance combined with its small form factor, inherent stability and precise control capability of the CPMSL chip make it a promising pulse source for low noise and high frequency applications, such as high speed communication systems, photonic assisted sampling, interchip/intrachip optical interconnects and clock distribution.

Funding

DARPA MTO DODOS contract (HR0011-15-C-055).

Acknowledgments

We thank Alexander W. Fang, Michael L. Davenport, Zeyu Zhang, Duanni Huang and Minh Tran for their helpful discussions. This research was developed with funding from the Defense Advanced Research Projects Agency (DARPA). The views, opinions and/or findings expressed are those of the author and should not be interpreted as representing the official views or policies of the Department of Defense or the U.S. Government.